Applied Materials Today 13 (2018) 303–309

Contents lists available at ScienceDirect

Applied Materials Today

journal homepage: www.elsevier.com/locate/apmt

Short communication

Pollen-inspired microparticles with strong adhesion for drug delivery

Yuetong Wang[a,b,1], Luoran Shang[a,1], Guopu Chen[c], Changmin Shao[a], Yuxiao Liu[a], Peihua Lu[b,**], Fei Rong[a,d,*], Yuanjin Zhao[a,b,*]

[a] State Key Laboratory of Bioelectronics, School of Biological Science and Medical Engineering, Southeast University, Nanjing 210096, China
[b] Department of Medical Oncology, Wuxi People's Hospital, Nanjing Medical University, Wuxi 214023, China
[c] Department of General Surgery, Jinling Hospital, Medical School of Nanjing University, Nanjing 210002, China
[d] Laboratory of Environment and Biosafety, Research Institute of Southeast University in Suzhou, Suzhou 215123, China

ARTICLE INFO

Article history:
Received 15 August 2018
Received in revised form
17 September 2018
Accepted 27 September 2018

Keywords:
Microparticles
Surface textures
Adhesion
Drug delivery

ABSTRACT

Microparticles with strong adhesion property was presented as efficacious drug delivery systems. Here, inspired by natural pollen, polymer microparticles with surface textures and homogeneous size were fabricated through evaporation-induced interfacial instability of microfluidic droplets templates. The resultant particles exhibited controllable surface roughness and thus strong adhesion ability to the intestinal mucosa. Such particles were employed as novel drug carriers, which contributed to enhanced loading efficacy and controllable release kinetics, and were proved to increase therapeutic effectiveness through *in vivo* and *in vitro* tests, thus playing a potential role in sustained drug delivery, bioimaging, diagnostics, *etc*.

1. Introduction

Microparticles with different sizes, morphology, and surface properties are among the most promising systems for targeted and controlled drug delivery and noninvasive drug administration [1–5]. By encapsulating therapeutic agents into microspheres or microcapsules, these particles serve as vehicles for the delivery of proteins, peptides, and small molecule drugs [6–14]. Fabrication of drug-loaded microparticles could be achieved through emulsion droplets templates, which are conventionally derived by various approaches including mechanically stirring [15], membrane emulsification [16], sonication [17], *etc*. However, particles obtained from these methods typically show high polydispersity, which are not conducive to controlling the amounts of drug loading and verifying the kinetics of drug release, therefore imposing limitations on the wide applications of these drug-loaded particles [18–20]. Besides, current drug microcarriers possess relatively simple surface structure and lack certain physicochemical properties and functions, such as adhesion ability [21–23]. This reduces drug delivery efficiency because insufficient adhesion of the carriers to the target results in rapid decrease of drug concentration and thus low sustainability [24]. Therefore, generating microparticles with homogeneous size distribution and strong adhesion property is highly in demand for constructing efficient drug delivery systems.

Natural plant pollen has emerged as promising micro-carriers for drug encapsulation [25]. In this paper, inspired by the strong adhesion of pollen to the respiratory tract and interactions with mucosa due to its coarse surface morphology (Fig. 1a) [26,27], we present a novel biodegradable particles with tunable surface textures as adhesive drug carriers via microfluidics, as shown in Fig. 1b. Due to their capability of generating monodisperse droplet templates and executing precise control over the physical and chemical processes during particles formation, microfluidic technology has become a crucial tool for controllable fabrication of microparticles with complex structures and desired functions [28–36]. However, microfluidic fabrication of microparticles with strong adhesion function for drug delivery is seldom reported. Herein, we used microfluidics to generate uniform droplets containing biocompatible polymers and a volatile solvent. Along with the evaporation of the solvent, shrinking droplets triggered interfacial instabilities to shape into microparticles with surface textures, the roughness of which could be controlled through various parameters. Adhesion ability tests showed that the stickiness of the particles displays a substantial positive correlation with surface roughness. These particles were then employed as carriers by loading drugs into the

* Corresponding authors at: State Key Laboratory of Bioelectronics, School of Biological Science and Medical Engineering, Southeast University, Nanjing 210096, China.
** Corresponding author.
E-mail addresses: lphty1_1@163.com (P. Lu), rong@seu.edu.cn (F. Rong), yjzhao@seu.edu.cn (Y. Zhao).
[1] These authors contributed equally to this work.

https://doi.org/10.1016/j.apmt.2018.09.016
2352-9407/

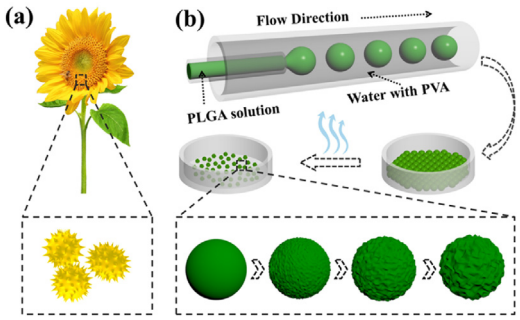

Fig. 1. Schematic illustration of (a) micromorphology of pollen from sunflower; (b) W/O droplets generated from a capillary microfluidic system and the fabrication process of microparticles with rough surface textures.

polymer matrix and were further interacted with human colon cancer cells and intestinal inflammation sites, respectively. The results from *in vitro* studies revealed that the porous rough surface morphography of microparticles could fast and durably release drugs to inhibit tumor cell growth. Meanwhile, *in vivo* studies reflected the strong adhesion of drug-loaded microparticles and hollows on their surface synergistically acted on attenuating symptoms of Crohn's disease. Also, convenience on controlling pharmacokinetics at the lesions makes these microparticles potentially ideal for sustained drug delivery, bioimaging, biodiagnostics, *etc*.

2. Results and discussion

In a typical experiment, monodisperse oil-in-water (O/W) droplets were generated by a capillary microfluidic device, which was assembled by coaxially aligning two (inner and outer) cylindrical capillaries inside a square capillary, as schematically depicted in Fig. 1b. The inner phase was an oil solution containing a blend of poly(lactic-co-glycolic acid) (PLGA) and diblock copolymers of poly(lactic-co-glycolic acid) and poly(ethylene glycol) (PLGA-b-PEG) dissolved in dichloromethane (DCM) and was infused through the inner capillary. The outer phase was an aqueous polyvinyl alcohol (PVA) solution and flowed via the interstices between the square capillary and the outer capillary. PVA here served as a surfactant to prevent droplets coalescence. When the two fluid phases met at the tip of the outer capillary, the inner oil phase was sheared into droplets by the outer water phase stream to form monodispersed O/W emulsions (Fig. 2a and b). These emulsion droplets were collected into a designed glass dish containing moderate PVA aqueous solution.

After collection, the organic solvent DCM in the droplets was evaporated and the droplets gradually shrank. This process triggered interfacial instabilities to form monodispersed pollen-like surface-textured microparticles, as shown in Fig. 2c. The removal of organic solvent remarkably improved the concentration of dissolved amphiphilic block copolymers. As a result, the oil/water interface became dramatically corrugated with many wrinkles extruded out from the droplets (Fig. S1). The influence of flow rates on the droplets' dimensional parameters was investigated, as shown in Fig. 2d and e. The droplets enlarged with increasing inner flow rate and decreasing outer flow rate. Meanwhile, ratio of block copolymers in blends impacted the flow rates because more PLGA would enhance the viscosity of inner phase. Under same set of flow rates, fluid possessing higher viscosity would be emulsified into larger droplets due to less shear force pushing the liquid forward and relatively stronger interfacial tension pulling the drops back [36]. As a result, the size of the microparticles obtained after complete evaporation of DCM was larger accordingly. In addition, the microparticles were highly monodispersed, with size dispersity of 4.89%, regardless of the inner and outer flow rates (Fig. 2f).

The degree of wrinkles such as protrusion length on the microparticles can be regulated by tuning the proportion of PLGA and PLGA-b-PEG in blends. If the total concentration of polymer mixture in the inner phase was kept constant, increasing the proportion of PLGA-b-PEG resulted in distinct improvement of surface wrinkles. The microstructures of various surface-textured microparticles were characterized using optical microscopy and scanning electron microscopy (SEM) (Fig. 3). When the PLGA-b-

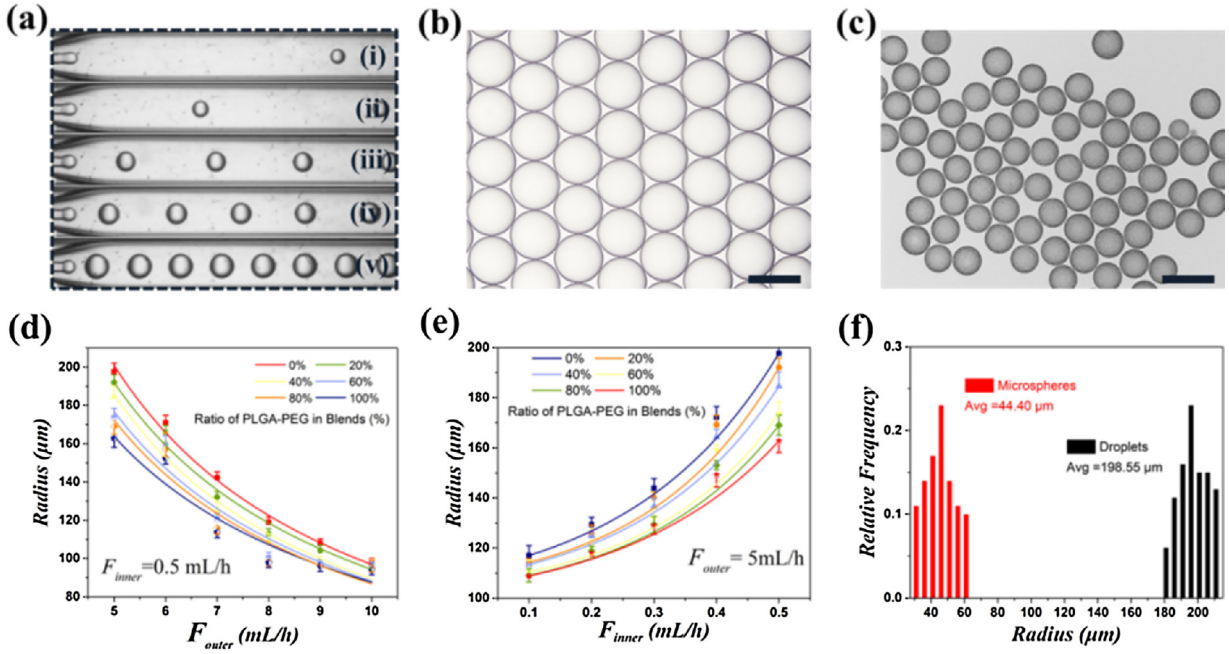

Fig. 2. (a) Real-time images of droplet emulsification in the microfluidic device with same outer flow rate at 5 mL/h and different inner flow rates at (i) 0.05 mL/h, (ii) 0.1 mL/h, (iii) 0.3 mL/h, (iv) 0.5 mL/h, and (v) 1.5 mL/h, respectively. (b and c) Microscope photographs of the (b) droplets and (c) solid pollen-like microparticles; the scale bars are 200 μm in (b) and 100 μm in (c), respectively. (d and e) Relationships of the microparticles radius with (d) the outer flow rate and (e) the inner flow rate, respectively. Error bars represent standard deviations. (f) The statistical size distribution of typical droplets and microparticles obtained after evaporation.

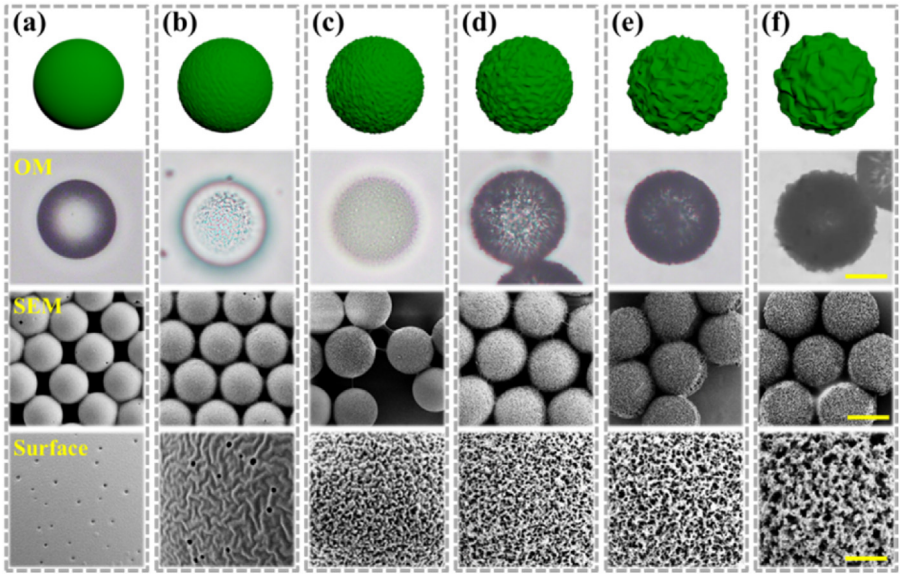

Fig. 3. Scheme, optical microscopy and SEM images of the microparticles containing PLGA-b-PEG/PLGA blends generated from microfluidic droplet templates. The ratios of PLGA-b-PEG in the blends were as follows: (a) 0%; (b) 20%; (c) 40%; (d) 60%; (e) 80%; and (f) 100%. The bottom row showed the amplified surface structure of these microparticles. The scale bars are 20 μm, 40 μm, and 8 μm for each row, respectively.

PEG was absent (which means the ratio of PLGA in the blends was 100%) the resultant microparticles had smooth surfaces, on which sparse holes were distributed, whose size ranged from 400 nm to 1 μm. When the PLGA-b-PEG content increased, protrusions emerged and gradually evolved into different morphologies. In particular, twisty strip wrinkles appeared on the particles surface when the PLGA-b-PEG content reached 20%. Such wrinkles then shifted to grain bulges at the value of 40%, followed by a deformation into a sheet-like texture with controllable protrusion lengths when this value approached 60% and above. Ultimately, with all PLGA-b-PEG, the length of the surface protuberances could reach approximately 10 μm. Meanwhile, the porosity of these particles dramatically improved with the enhancement of surface textures. This was demonstrated by characterization of the particles surface areas through Brunauer–Emmett–Teller (BET) measurements, as shown in Fig. S2. The formation of such porous microparticles with rough surface morphologies could be explained by phase separation and interfacial instability mechanism [37–39]. During the removal of the volatile DCM solvent, the droplets shrank and the polymer viscosity increased. As a result, phase-separation occurred in the PEG-rich interface, which contributed to the porous structure and highly corrugated surface morphology. The phase separation was originated from the intrinsic incompatibility between PLGA and PEG, and the consequent need to reduce the interfacial area [15]. The more PLGA-b-PEG existed in the blends, the fiercer surface roughening proceeded. Thus, microparticles with controllable surface textures can be achieved simply by tuning ratio of PLGA-b-PEG in blends.

The adhesion ability of these surface textured microparticles was verified through *in vivo* testing on the colon epithelium in the Sprague–Dawley (SD) rats, who received an enema with six kinds of textured microparticles with different surface morphologies. By counting remaining microparticles in the intestinal tract, the adhesion rate was calculated. Enemas containing aforesaid polymer microparticles resulted in prominent adherence, and particles with different degrees of surface roughness exhibited distinct adhesion behaviors. As illustrated in Fig. 4b and c, the stickiness of the microparticles displays a substantial positive correlation with surface roughness. The total proportion of remaining microparticles with neat PLGA (0.538) was markedly lower than that of the PLGA-b-PEG group (0.957). In addition, highly-textured microparticles, like when the proportion of PLGA-b-PEG reached 60% and above, had a greater probability to adhere to the forepart of the colon mucosa. On the contrary, particles with relatively less surface structures tended to creep down to the middle and back segments. As shown from the adhesion rate chart (Fig. 4b), ratio of microparticles retentive within 0.5–1.5 cm and 3.5–4.5 cm of the colon severally escalated and declined, along with the increase of surface roughness. Compared with smooth microparticles, greater coarseness derived from wrinkles and projections on the textured particles surface account for their preferential adhesion to colon mucosa. It was worth mentioning that, to extend the function of these textured microparticles, oil-soluble Fe_3O_4 nanoparticles could be incorporated into the inner phase during droplets generation. Therefore, the resultant microparticles were endowed with magnetic responsiveness feature, as shown in Fig. S4. Such biocompatible, highly adhesive, and magneto-responsive microparticles would thereby provide a potential reservoir for prolonged local drug availability and improved therapeutic efficacy.

To demonstrate the potential value of the surface textured microparticles, their performances as drug delivery systems were investigated through *in vitro* experiments, as shown in Fig. 5. In specific, the hydrophobic broad-spectrum anticancer drug, camptothecin (CPT), was dissolved at a moderate concentration into inner oil phase of the microfluidic droplet templates. During particles generation, the oil-soluble drug molecules were locked in the solidified PLGA and PLGA-b-PEG polymer networks with high encapsulation efficiency while without hampering the formation of surface textures. The microparticles were separated from the collection solution and soon dried after purification. They could be preserved for a long time while maintaining good encapsulation efficacy. The dispersion of the self-fluorescent CPT was observed directly under the confocal laser scanning microscopy (CLSM), which showed uniform distribution throughout the PLGA and PLGA-b-PEG mixture, indicating efficient drug loading capacity of the microparticles (Fig. S3).

Quantitative encapsulation efficiency (EE%) and drug loading (DL%) of CPT in microparticles were measured, and clearly the extent of surface textures significantly affected the EE% and DL%,

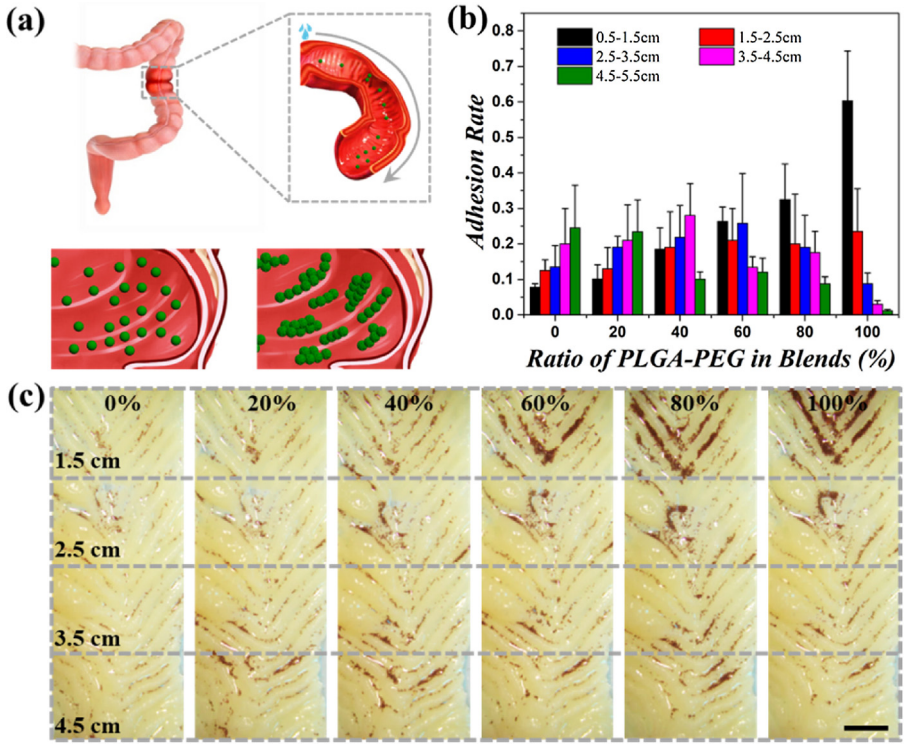

Fig. 4. (a) Schematic diagram of the process of adhesion test and the adherence distinction between smooth and highly-textured microparticles; (b) statistical ratio of microparticles retentive at different colon segments calculated by counting method. The total proportion of remaining microparticles in the intestinal tract for different ratios of PLGA-b-PEG in the blends were as follows: 0%: 0.538; 20%: 0.632; 40%: 0.873; 60%: 0.866; 80%: 0.891; 100%: 0.957; (c) optical microscopy images of microparticles with various degrees of surface textures adhering to different colon segments. The scale bar is 0.5 cm.

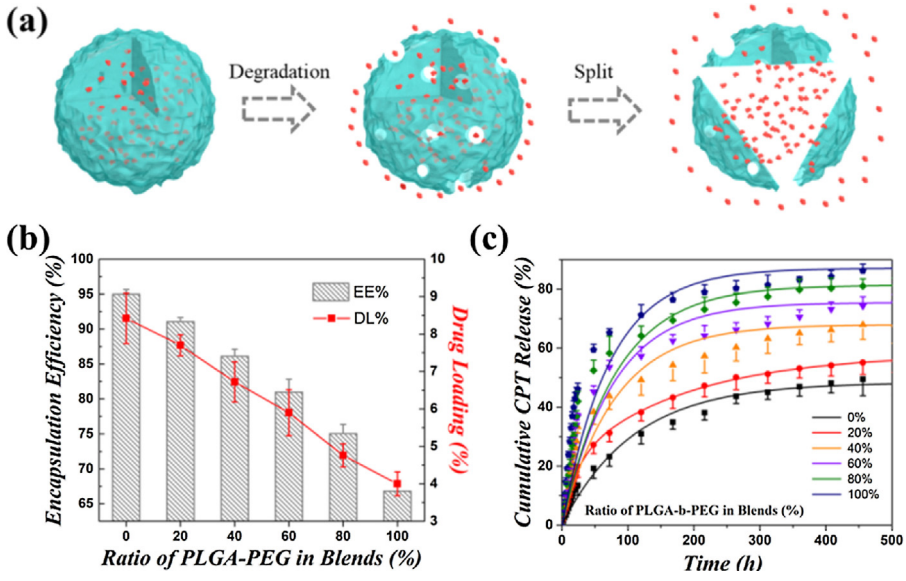

Fig. 5. (a) Schematic illustration of the microparticle degradation and drug release; (b) EE% and DL% of CPT for particles with different relative PLGA-b-PEG/PLGA contents; (c) The cumulative percentage release curves of CPT from the microparticles with different relative PLGA-b-PEG/PLGA contents.

as depicted in Fig. 5b. Eqs. (1) and (2) [38] shows how EE% and DL% were calculated.

$$\text{EE\%} = \frac{\text{amount of drug encapsulated}}{\text{total amount of drug used}} \times 100 \quad (1)$$

$$\text{DL\%} = \frac{\text{amount of drug loaded}}{\text{amount of polymer}} \times 100 \quad (2)$$

In the case of neat PLGA, the encapsulation efficiency reached a highest value of 95.0 ± 0.64%. The incomplete encapsulation might be resulted from trace loss of the CPT, which was taken out of the particles via the random-distributed surface pores during the DCM evaporation process. As the amount of PLGA-b-PEG increased, the value of EE% declined, which reached a minimum of 66.8 ± 1.0% in the case of neat PLGA-b-PEG particles. The reasons can be ascribed to the diminution of hydrophobic component and reinforced porous structure of microparticles. The reduction of PLGA content provided relatively less hydrophobic domain in the polymer network for the loading of the hydrophobic CPT. Meanwhile,

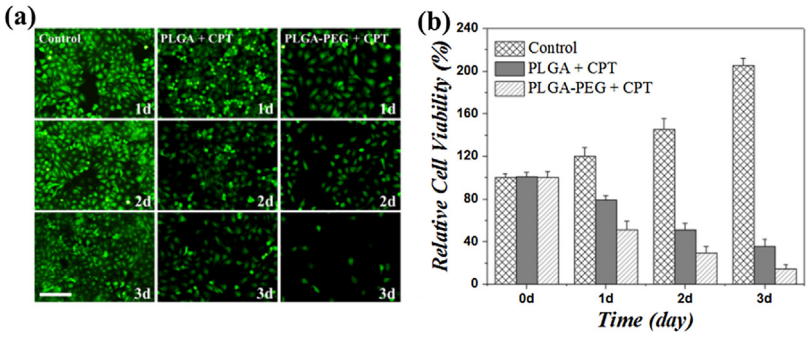

Fig. 6. (a) Fluorescent images of HCT-116 cells treated by drug-free microparticles, CPT-loaded PLGA microparticles, and CPT-loaded PLGA-b-PEG microparticles. The scale bar is 20 μm. (b) Corresponding viability of HCT-116 cells cultured in the different groups.

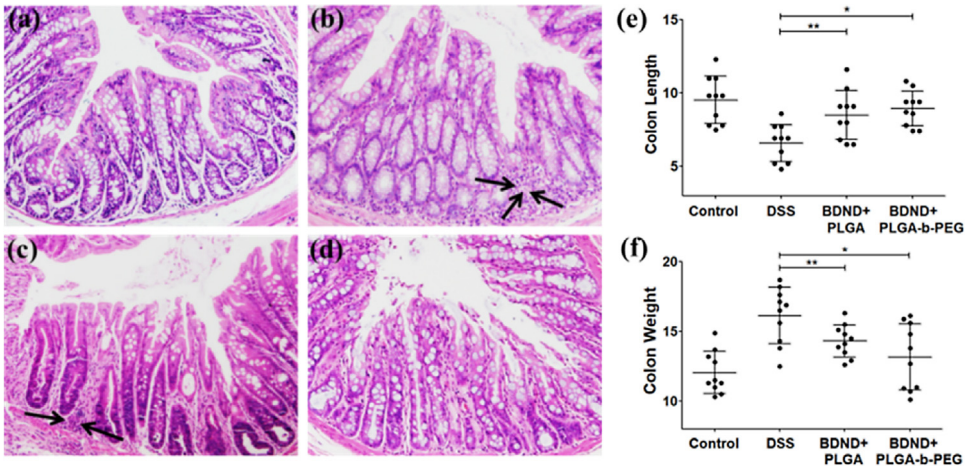

Fig. 7. Hematoxylin and eosin (H&E) histology images of the different mice groups. (a) Control mice received no treatment. (b) Mice with DSS-induced Crohn receiving no treatment. (c and d) Mice with Crohn's disease treated with enema of (c) pure BUD-loaded PLGA and (d) PLGA-b-PEG microparticles. (e and f) Colon (e) length and (f) weight measured in the second independent experiment. Data were means ± SD (n = 10 mice per group). P values were determined by one-way ANOVA with Tukey post hoc test.

more hollows on the surface accelerated drug leakage, which contributed to the quick fall of EE%.

To investigate the release kinetics of CPT, the drug-loaded polymer particles were emerged in phosphate buffered saline (PBS, pH 7.4) solution at 37 °C to mimic the human physiological environment. As shown in Fig. 5a, CPT could be released gradually with the degradation of the polymer. Fig. S5 showed that the more PLGA-b-PEG occupied, the more quickly microparticles degraded. The cumulative release profile of CPT from different surface textured microparticles is displayed in Fig. 5c. It showed an initial burst in the first 24 h, followed by a continuous profile and eventually reached the maximum. The initial burst release could be attributed to the escape of the loosely encapsulated drug from the microparticles' polymer matrix. After that, the long-term steady process indicated a sustainable release profile, and the CPT release was accelerated with the increase of surface roughness. This was a result of higher surface area of the porous microparticles, which made them more favorable for water adsorption and hence enhanced wettability [39], thus leading to an increased release. Therefore, by tailoring the extent of surface roughness, the drug loading and release kinetics can be effectively controlled.

The advantage of the porous and rough surface of PLGA-b-PEG microparticles was embodied in enhancing therapeutic effect of the anticancer drug. The CPT-loaded microparticles were interacted with human colon cancer cells, HCT-116. CPT is a cytotoxic quinolone alkaloid that can inhibit DNA enzyme topoisomerase I, prevent DNA re-ligation, and cause DNA damage, thus resulting in apoptosis [40]. Here, HCT-116 cells were incubated for 3 days with unloaded microparticles, CPT-loaded PLGA microparticles, and CPT-loaded PLGA-b-PEG microparticles with an equivalent CPT dosage, respectively. Optical and fluorescence images in Fig. 6a showed that the HCT-116 cells grew well in the culture plate with presence of drug-free microparticles (set as the control group), indicating excellent biocompatibility of the polymer materials. However, the viability of HCT-116 cells incubated with CPT loaded microparticles was lower than that of the control group, and it decreased with incubation time. Comparing these two kinds of drug-loaded microparticles, the cell viability of the PLGA-b-PEG group was lower than that of the PLGA group. After incubation for 3 days, the total apoptotic HCT-116 cell populations in the PLGA-b-PEG group (85.88%) is remarkably higher than the PLGA group (64.77%), as shown in Fig. 6b. These results indicated that, those porous drug carrier microparticles with highly textured surfaces could significantly reduce cell viability, and enhance therapeutic efficacy in treating cancer cells, compared with the relatively smooth carriers, which corresponded to the results of drug release curves above.

The synergistic effect of drug-loaded adhesive microparticles' strong adhesion and multihole structure was examined using dextran sulfate sodium (DSS) modeling. Budesonide (BUD) is a medication of the corticosteroid type, which can be delivered in rectal form for inflammatory bowel disease including Crohn's disease, ulcerative colitis and microscopic colitis [41]. Here, mice received an enema of BUD-loaded polymer microparticles with neat PLGA and neat PLGA-b-PEG, respectively. Untreated mice and mice with Crohn modeling using dextran sulfate sodium (DSS) were set as

controls. Crohn disease was characterized by infiltration of the colon lamina propria with neutrophils and mononuclear inflammatory cells, crypt hypertrophy, and superficial erosions [42]. Results showing in Fig. 7a and d demonstrated that histological inflammation was diminished in the mice treated with two BUD-loaded microparticles, and the disease severity was significantly reduced in mice given BUD-loaded PLGA-b-PEG microparticles compared to that of the PLGA experimental group. Colon length and weight were scored as additional statistically significant parameters for disease activity. It is noted that Crohn disease will cause length shortening and weight gaining of the colon. As shown in Fig. 7e and f, there was a more notable statistic difference between DSS group and BUD+ PLGA-b-PEG group on the colon length ($P = 0.0004$) and weight ($P = 0.0077$) compared with BUD+ PLGA group. The results indicated that administration of BUD-loaded microparticles had therapeutic impact on recovering normal colon to some extent. Especially, PLGA-b-PEG microparticles performed better by virtue of their stronger adhesion and more efficient drug delivery. These features of the microparticles indicated their potential value as functional delivery systems.

3. Conclusion

In summary, we have developed novel drug delivery microparticles with uniform size, controllable surface textures and strong adhesion through microfluidic droplets templates. Surface textures were generated during particles formation due to evaporation-induced interfacial instability. The degree of particles roughness could be controlled simply by adjusting the component ratio of polymer blends in the droplets. Strong adhesion ability of the resultant particles was confirmed through *in vivo* testing on the colon epithelium. Such adhesive particles were served as drug delivery vehicles with good biocompatibility, high loading efficiency, controllable release kinetics, and strong adhesion. These advantages contributed to improved therapeutic efficacy of the particles for inflammatory Crohn's disease, indicating potential role of the particles in fields of sustained drug delivery, bioimaging, biodiagnostics, *etc*.

Acknowledgements

This work was supported by the National Key Research and Development Program of China (2017YFA0700404), the National Natural Science Foundation of China (grants 51522302 and 21473029), the NSAF Foundation of China (grant U1530260), the Fundamental Research Funds for the Central Universities, the Scientific Research Foundation of Southeast University, the Scientific Research Foundation of Graduate School of Southeast University, and the Innovation Program for Agricultural Science and Technology of Suzhou (SNG201603).

Appendix A. Supplementary data

Supplementary data associated with this article can be found, in the online version, at doi:10.1016/j.apmt.2018.09.016.

References

[1] I.G. Loscertales, A. Barrero, I. Guerrero, R. Cortijo, M. Marquez, A.M. Gañán-Calvo, Micro/nano encapsulation via electrified coaxial liquid jets, Science 295 (2002) 1695.
[2] S.H. Kim, H.C. Shum, J.W. Kim, J.C. Cho, D.A. Weitz, Multiple polymersomes for programmed release of multiple components, J. Am. Chem. Soc. 133 (2011) 15165.
[3] H. Lv, Q. Lin, K. Zhang, K. Yu, T.J. Yao, X.H. Zhang, J.H. Zhang, B. Yang, Facile fabrication of monodisperse polymer hollow spheres, Langmuir 24 (2008) 13736.
[4] W. Cui, Y. Zhou, J. Chang, Electrospun nanofibrous materials for tissue engineering and drug delivery, Sci. Technol. Adv. Mater. 11 (2010) 014108.
[5] I. Sargin, L. Akyuz, M. Kaya, G. Tan, T. Ceter, K. Yildirim, S. Ertosun, G.H. Aydin, M. Topal, Controlled release and anti-proliferative effect of imatinib mesylate loaded sporopollenin microcapsules extracted from pollens of *Betula pendula*, Int. J. Biol. Macromol. 105 (2017) 749.
[6] R. Langer, Drug delivery and targeting, Nature 392 (1998) 5.
[7] O.L. Johnson, J.L. Cleland, H.J. Lee, M. Charnis, E. Duenas, W. Jaworowicz, D. Shepard, A. Shahzamani, A.J. Jones, S.D. Putney, A month-long effect from a single injection of micro-encapsulated human growth hormone, Nat. Med. 3 (1996) 795.
[8] H.C. Shum, J.W. Kim, D.A. Weitz, Microfluidic fabrication of monodisperse biocompatible and biodegradable polymersomes with controlled permeability, J. Am. Chem. Soc. 130 (2008) 9543.
[9] P. Wang, L. Zhang, W. Zheng, L. Cong, Z. Guo, Y. Xie, L. Wang, R. Tang, Q. Feng, Y. Hamada, K. Gonda, Z. Hu, X. Wu, X. Jiang, Thermo-triggered release of CRISPR-Cas9 system by lipid-encapsulated gold nanoparticles for tumor therapy, Angew. Chem. Int. Ed. Engl. 6 (2018) 1491.
[10] S. Zhou, X. Deng, H. Yang, Biodegradable poly(epsilon-caprolactone)-poly(ethylene glycol) block copolymers: characterization and their use as drug carriers for a controlled delivery system, Biomaterials 24 (2003) 3563.
[11] D. Wang, A. Rogach, F. Caruso, Semiconductor quantum dot-labeled microsphere bioconjugates prepared by stepwise self-assembly, Nano Lett. 8 (2002) 857.
[12] L. Zhang, Q. Feng, J. Wang, J. Sun, X. Shi, X. Jiang, Microfluidic synthesis of rigid nanovesicles for hydrophilic reagents delivery, Angew. Chem. Int. Ed. Engl. 54 (2015) 3952.
[13] M.A. Shahbazi, M. Hamidi, E.M. Mäkilä, H. Zhang, P. Almeida, M. Kaasalainen, J.J. Salonen, J.T. Hirvonen, H.A. Santos, The mechanisms of surface chemistry effects of mesoporous silicon nanoparticles on immunotoxicity and biocompatibility, Biomaterials 31 (2013) 7776.
[14] M. Mujtaba, I. Sargin, L. Akyuz, T. Ceter, M. Kaya, Newly isolated sporopollenin microcages from *Platanus orientalis* pollens as a vehicle for controlled drug delivery, Mater. Sci. Eng. C 77 (2017) 263.
[15] H.J. Chung, K.K. Hong, J.J. Yoon, T.G. Park, Heparin immobilized porous PLGA microspheres for angiogenic growth factor delivery, Pharm. Res. 8 (2006) 1835.
[16] S.V.D. Graaf, C.G.P.H. Schroën, R.M. Boom, Preparation of double emulsions by membrane emulsification—a review, J. Membr. Sci. 251 (2005) 7.
[17] E. Campos, J. Branquinho, A.S. Carreira, A. Carvalho, P. Coimbra, P. Ferreira, M.H. Gil, Designing polymeric microparticles for biomedical and industrial applications, Eur. Polym. J. 49 (2013) 2005.
[18] F. Fu, L. Shang, F. Zheng, Z. Chen, H. Wang, J. Wang, Z. Gu, Y. Zhao, Cell cultured on core–shell photonic crystal barcodes for drug screening, ACS Appl. Mater. Int. 8 (2016) 13840.
[19] Y. Yin, A.P. Alivisatos, Colloidal nanocrystal synthesis and the organic–inorganic interface, Nature 437 (2005) 664.
[20] Y. Li, D. Yan, F. Fu, Y. Liu, B. Zhang, J. Wang, L. Shang, Z. Gu, Y. Zhao, Composite microparticles from microfluidics for synergistic drug delivery, Sci. China Mater. 60 (2017) 543.
[21] F. Fu, L. Shang, Z. Chen, Y. Yu, Y. Zhao, Bioinspired living structural color hydrogels, Sci. Robot. 3 (2018) eaar8580.
[22] L.M. Bimbo, E. Mäkilä, T. Laaksonen, V.P. Lehto, J. Salonen, J. Hirvonen, H.A. Santos, Drug permeation across intestinal epithelial cells using porous silicon nanoparticles, Biomaterials 32 (2011) 2625.
[23] Y. Liu, Q. Huang, J. Wang, F. Fu, J. Ren, Y. Zhao, Microfluidic generation of protein biomedical microcarriers, Sci. Bull. 62 (2017) 1283.
[24] B. Sarmento, A. Ribeiro, F. Veiga, P. Sampaio, R. Neufeld, D. Ferreira, Alginate/chitosan nanoparticles are effective for oral insulin delivery, Pharm. Res. 24 (2007) 2198.
[25] L. Akyuz, I. Sargin, M. Kaya, T. Ceter, I. Akata, A new pollen-derived microcarrier for pantoprazole delivery, Mater. Sci. Eng. C 71 (2016) 937.
[26] M.J. Uddin, H.S. Gill, Ragweed pollen as an oral vaccine delivery system: Mechanistic insights, J. Control. Release 268 (2017) 416.
[27] M.G. Potroz, R.C. Mundargi, J.J. Gillissen, E. Tan, S. Meker, J.H. Park, H. Jung, S. Park, D. Cho, S. Bang, N. Cho, Drug delivery: plant-based hollow microcapsules for oral delivery applications: toward optimized loading and controlled release, Adv. Funct. Mater. 31 (2017) 1700270.
[28] Y. Yu, F. Fu, L. Shang, Y. Cheng, Z. Gu, Y. Zhao, Bio-inspired helical microfibers from microfluidics, Adv. Mater. 29 (2017) 1605765.
[29] J. Wang, L. Sun, M. Zou, W. Gao, C. Liu, L. Shang, Z. Gu, Y. Zhao, Bioinspired shape-memory graphene film with tunable wettability, Sci. Adv. 3 (2017) e1700004.
[30] S. Wang, K. Liu, J. Liu, Z. Yu, X. Xu, L. Zhao, T. Lee, E.K. Lee, J. Reiss, Y.K. Lee, L.W. Chung, J. Huang, M. Rettig, D. Seligson, K.N. Duraiswamy, C.K. Shen, H.R. Tseng, Highly efficient capture of circulating tumor cells by using nanostructured silicon substrates with integrated chaotic micromixers, Angew. Chem. Int. Ed. Engl. 13 (2011) 2909.
[31] L. Shang, Y. Cheng, Y. Zhao, Emerging droplet microfluidics, Chem. Rev. 117 (2017) 7964.
[32] J.U. Shim, R.T. Ranasinghe, C.A. Smith, S.M. Ibrahim, F. Hollfelder, W.T. Huck, D. Klenerman, C. Abell, Ultrarapid generation of femtoliter microfluidic droplets for single-molecule-counting immunoassays, ACS Nano 7 (2013) 5955.
[33] H. Wang, Z. Zhao, Y. Liu, C. Shao, F. Bian, Y. Zhao, Biomimetic enzymes cascade reaction system in microfluidic electrospray microcapsules, Sci. Adv. 4 (2018) eaat2816.

[34] R. Vasiliauskas, D. Liu, S. Cito, H. Zhang, M.A. Shahbazi, T. Sikanen, L. Mazutis, H.A. Santos, Simple microfluidic approach to fabricate monodisperse hollow microparticles for multidrug delivery, ACS Appl. Mater. Int. 27 (2015) 14822.
[35] Y. Yu, L. Shang, W. Gao, Z. Zhao, H. Wang, Y. Zhao, Microfluidic lithography of bioinspired helical micromotors, Angew. Chem. Int. Ed. Engl. 56 (2017) 12127.
[36] Y. Song, C.T. Michaels, Q. Ma, Z. Liu, H. Yuan, S. Takayama, P.J. Knowles, H.C. Shum, Budding-like division of all-aqueous emulsion droplets modulated by networks of protein nanofibrils, Nat. Commun. 9 (2018) 2110.
[37] S. Liu, R. Deng, W. Li, J. Zhu, Polymer microparticles with controllable surface textures generated through interfacial instabilities of emulsion droplets, Adv. Funct. Mater. 22 (2012) 1692.
[38] M. Hussain, J. Xie, Z. Hou, K. Shezad, J. Xu, K. Wang, Y. Gao, L. Shen, J. Zhu, Regulation of drug release by tuning surface textures of biodegradable polymer microparticles, ACS Appl. Mater. Int. 16 (2017) 14391.
[39] X. Yu, Z. Zhao, W. Nie, R. Deng, S. Liu, R. Liang, K. Zhu, X. Ji, Biodegradable polymer microcapsules fabrication through a template-free approach, Langmuir 16 (2011) 10265.
[40] R.A. Shamanna, H. Lu, D. Croteau, A. Arora, D. Agarwal, G. Ball, M.A. Aleskandarany, I.O. Ellis, Y. Pommier, S. Madhusudan, V.A. Bohr, Camptothecin targets WRN protein: mechanism and relevance in clinical breast cancer, Oncotarget 7 (2016) 13269.
[41] D.A. Lipson, H. Barnacle, R. Birk, N. Brealey, N. Locantore, D.A. Lomas, A. Ludwig-Sengpiel, R. Mohindra, M. Tabberer, C.Q. Zhu, S.J. Pascoe, Fulfil trial: once-daily triple therapy in patients with chronic obstructive pulmonary disease, Am. J. Resp. Crit. Care 196 (2017) 438.
[42] S. Zhang, J. Ermann, M.D. Succi, A. Zhou, M.J. Hamilton, B. Cao, J.R. Korzenik, J.N. Glickman, P.K. Vemula, L.H. Glimcher, G. Traverso, R. Langer, J.M. Karp, An inflammation-targeting hydrogel for local drug delivery in inflammatory bowel disease, Sci. Transl. Med. 300 (2015) 300ra128.